MLF Experimental Report	提出日 Date of report
実験課題番号 Project No. 2014P0601 実験課題名 Title of experiment Development of fundamental techniques for pulsed neutron imaging 実験責任者名 Name of principal investigator Yoshiaki Kiyanagi 所属 Affiliation Nagoya University	装置責任者 Name of responsible person Kenichi Oikawa 装置名 Name of Instrument/（BL No.） NOBORU /(BL10) 利用期間 Dates of experiments 22/May/2014 – 26/May/2014 26/May/2014 – 28/May/2014 29/May/2014 – 1/June/2014 7/June/2014 – 9/June/2014 18/June/2014 – 20/June/2014 8/Apr/2015 – 10/Apr/2015 11/Apr/2015 – 13/Apr/2015 13/Apr/2015 – 15/Apr/2015 25/Apr/2015 – 27/Apr/2015

1．研究成果概要（試料の名称、組成、物理的・化学的性状を明記するとともに、実験方法、利用の結果得られた主なデータ、考察、結論、図表等を記述してください。

Outline of experimental results (experimental method and results should be reported including sample information such as composition, physical and/or chemical characteristics.

I. Bragg edge imaging

I. 1 Bragg-edge measurement for the crystallite size, and the crystalline orientation analysis of Japanese sword.

(1) Purpose

The purpose is Bragg-edge measurement of Japanese sword for crystallite size distribution crystalline orientation analysis.

(2) Background

We have continued to apply the Bragg edge imaging technique to a Japanese sword study. The crystallite size distribution and crystalline orientation distribution are important information for considering sword manufacturing techniques. This crystallographic information is obtained by a total fitting of a Bragg edge spectrum with high statistics over wide wavelength region. Therefore, we measured Bragg-edge spectrum of a Japanese sword by using a high counting type detector.

(3) Experimental

GEM detector was set at 14.5m flight path length position on the sample table of BL10. The sample was a short type Japanese sword, and was named “Bizen-Osafune-no-Ju-Norimitsu”. 4 transmission measurements were performed at 4 squire areas shown in Fig. 1. Crystalline orientation and crystallite size were obtained from the neutron transmission spectrum fitting with the use of the RITS program.

(4) Preliminary Result

Fig. 2 shows a neutron transmission image and a crystallite size mapping at sword tip. Small sized crystallite was distributed evenly over blade area, due to homogeneous forging (shaping metal by hammering and heating). And, crystallite size became smaller from center to blade due to martensite with high micro strain. Crystalline orientation was shown in Fig. 3 as an orientation parameter R_{hkl} that is the coefficient of March-Dollase-function. Anisotropic crystalline orientation was observed at the back position of sword blade. On the other hand, isotropic crystalline orientation was observed at the middle position of sword grip.

As a result, differences in the crystallographic structure were observed depending on the locations in the sword, i.e. the blade, back side, grip, etc.

Such a metallographic information depends on carbon content in steel, forging condition, quenching to harden the blade, and processing temperature. Bragg edge analysis will be a profitable tool for metallographic structure research of Japanese sword in a non-destructive way.

Fig. 1 Photograph of the Japanese sword with neutron transmission measurement areas.

1．研究成果概要（つづき） Outline of experimental results (continued).

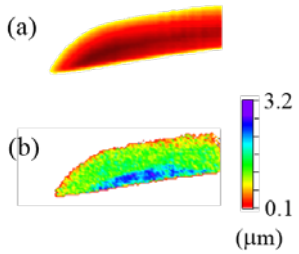

Fig. 2 Neutron imaging (a) and crystallite size mapping at sword tip.

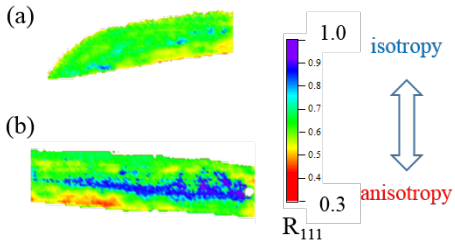

Fig. 3 Crystalline orientation mapping of sword tip (a) and sword grip (b).

I. 2 Crystal orientation mapping for a large grain material.

(1) Background

Mapping of crystal orientation and crystalline grains in a material is one of important expressions of material characteristics. Electron backscatter diffraction and X-ray diffraction imaging are conventional methods for grain orientation mapping. However, it is difficult for these techniques to evaluate bulk information of steels. Therefore, neutron diffraction imaging is expected as a new method for the bulk steel analysis. However, spatial resolution of the diffraction imaging is lower than that of transmission imaging. Thus, we developed grain orientation mapping method using neutron transmission imaging technique. In this experiment, we tried to map grain orientation by position-dependent data analysis of neutron transmission spectra including Bragg scattering information.

(2) Experiment

The sample was 3.4mass% Si-steel plate of 5 mm thickness and about 7 cm x 7 cm area. This sample contained mm/cm-order crystalline grains. Position-dependent neutron transmission spectra of the sample were obtained by using the nGEM detector. Fig. 4 shows examples of wavelength-dependent neutron transmission images and neutron transmission spectra. Grain images and single-crystal-type Bragg-dip transmission spectra were obtained. Finally, we deduced crystal orientation from the Bragg-dip transmission spectrum, and mapped the orientation position-dependently.

1．研究成果概要（つづき） Outline of experimental results (continued).

(3) Preliminary Result

Fig. 5 shows results of grain orientation mapping. In this sample, it was found that there is one grain or two grains in the path of neutron transmission through the evaluation of the Bragg-dip transmission spectra. Therefore, two images are presented. The same color between two images indicates single grain region. On the other hand, the different colors between two images indicates double grains region. Since this image covers whole region of the sample, it was found that the developed Bragg-dip transmission spectral analysis method can deal with the spectrum composed of several grains.

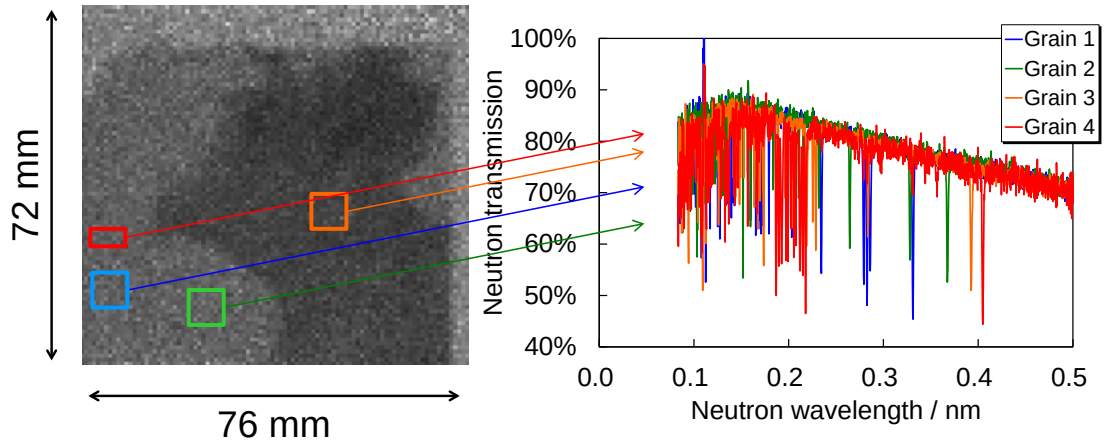

Fig. 4. (Left) Neutron radiography of 0.368 nm wavelength. (Right) Neutron transmission spectra with Bragg-dips due to single crystal.

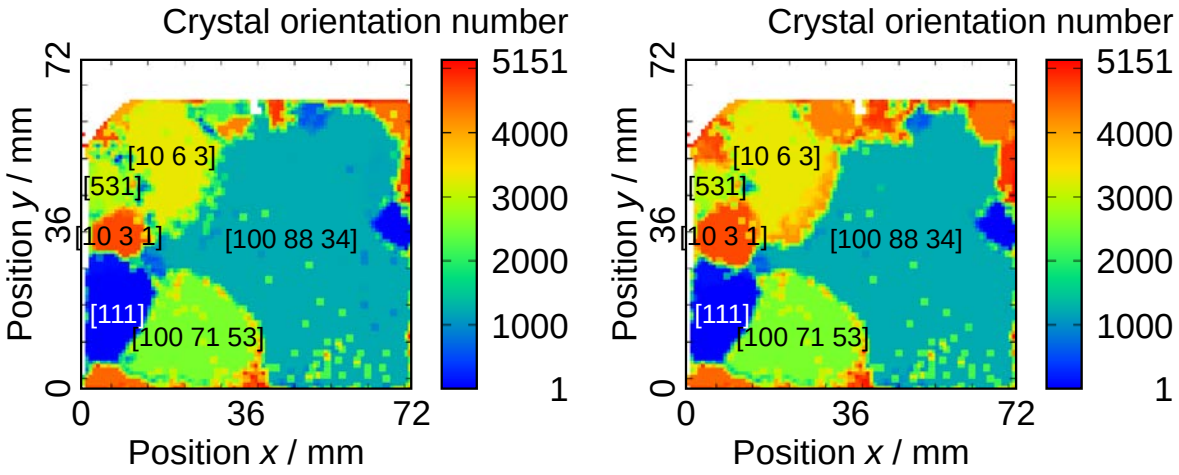

Fig. 5. (Left) Grain orientation mapping of single grain or first grain. (Right) Grain orientation mapping of single grain or second grain. [hkl] expresses crystal orientation Miller index.

I. 2 Temperature measurement using diffraction and Bragg-edge technique.

(1) Purpose

The purpose of this experiment was a feasibility study of temperature measurement by using diffraction and Bragg-edge technique.

(2) Background

Lattice constants of a crystalline material can be obtained by a diffractometry. A high-resolution neutron powder diffraction, $\Delta d/d \sim 10^{-3}$, provides precise lattice parameter, a, using a pattern fitting such as the Rietveld or the Pawley method, where achievable $\Delta a/a$ is under 10^{-4}. In contrast, a transmission spectrum through the crystalline sample shows a sharp saw-tooth shape, so called Bragg-edge, where the edge positions in wavelength λ are consistent with the Bragg peaks of $d_{hkl} = \lambda/2$. Sato *et al.* have developed a Rietveld-type analysis code for pulsed neutron Bragg-edge transmission spectra, RITS. The Bragg-edge analysis should have high-resolution capability, but corresponding $\Delta a/a$ is unclear up to now. Therefore we measured diffraction patterns and transmission spectra to evaluate the temperature distribution in heated Cu rod, and estimate the temperature from the refined lattice parameter in quasi-one dimensional data.

(2) Experiment

The pulsed neutron transmission imaging and the diffraction experiment were performed on the BL10 NOBORU at MLF/J-PARC. A copper rod, which was mounted on a heater-block, was set at about 14 m from the neutron source. Fig. 6 is a picture of the experimental setup around the sample. The transmission of the normal direction of the sample was obtained by measuring 2D spectra with and without the sample in front of a gas electron multiplier (GEM) detector. The diffraction data at $2\theta = 90^\circ$ was taken by the 1D position sensitive detectors (1D-PSDs) with a 16’ soller slit. Temperature distribution of the sample was monitored by thermocouples.

(3) Preliminary Result

Fig. 7 shows transmission spectra (left), diffraction patterns (center), and obtained expansion ratio of two methods (right). The refined values obtained using the two methods show similar trends; however, the accuracy of the transmission results seems lower than that of the neutron diffraction results in the present study. We have started reconsidering the statistical weighting of the raw transmission spectra used in the RITS code.

This work is partially supported by Photon and Quantum Basic Research Coordinated Development Program from the Ministry of Education, Culture, Sports, Science and Technology, Japan.

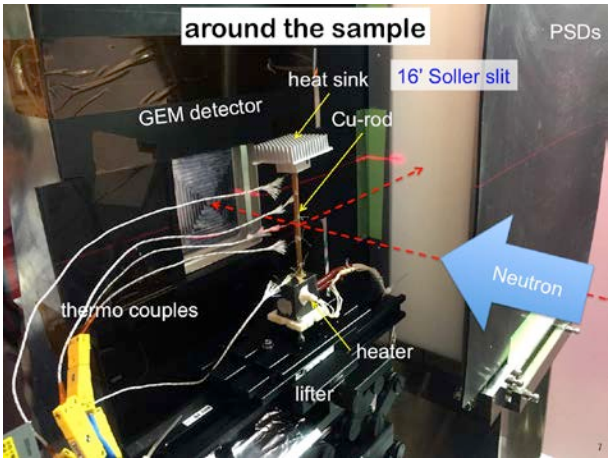

Fig. 6 Heated Cu rod, GEM detector and 1D-PSDs with a soller slit.

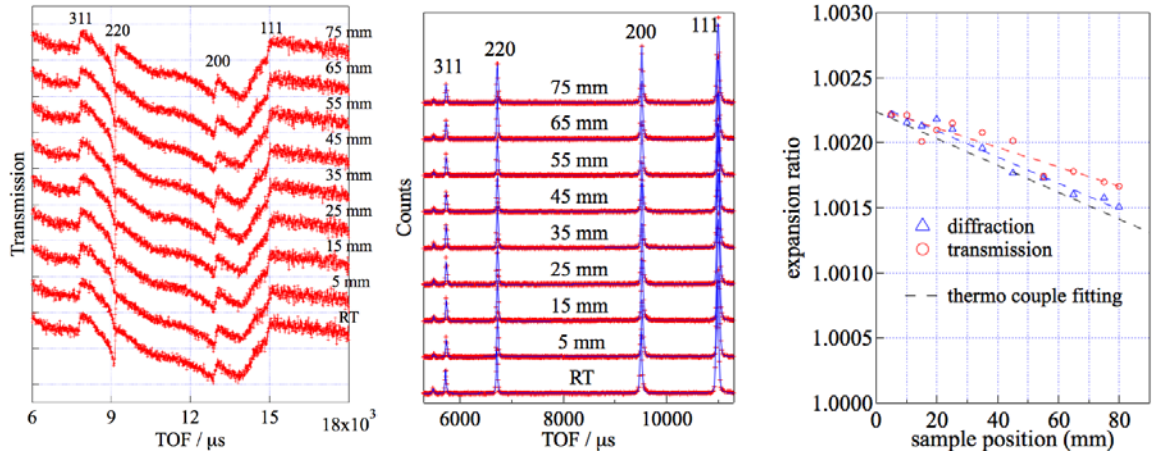

Fig. 7 Transmission spectra (left) and diffraction patterns (center) of heated Cu rod, and the obtained expansion ratios of both methods with those of thermocouple (right).

II. Resonance Imaging

II. 1 Resonance imaging of the different thickness sample.

(1) Experiment

Sample

1. Cu plate (thickness 1 mm)
2. Ag plate (thickness 1 mm)
3. Black resonance filter (Manganine 6 mm, W 0.7 mm, Ta 0.149 mm, Cd 0.25 mm)
4. Solder (Sn 96.5 %, Ag 3%, Cu 0.5%)

In the neutron resonance transmission measurements, the black resonance filter was used to estimate background due to scattered neutrons. We obtained transmission spectra of Cu and Ag plate and measured the background level using the filter in the cases of sample-in/out. The Gas Electron Multiplier (GEM) detector was used.

For the lead-free solder, we carried out imaging experiments using neutron resonance transmission. The solder consists of Sn (96.5%), Ag (3%) and Cu (0.5%). Thickness of the sample was 4.8 mm on the left side region and 3.2 mm on the right side region.

(2) Preliminary Result

Fig. 8 shows the TOF spectra of neutrons transmitted through the filter and background curves. The background curves were determined by fitting a line to the saturated resonance dips which represent the background level. The obtained transmission spectra were corrected using the background curves and then the atomic area densities of the samples were estimated. The area density of Ag plate was estimated at $(5.76 \pm 0.15) \times 10^{-3}$ atoms/barn (99.1% of actual density) from the fitting to the 71 eV resonance dip. On the other hand, the area density of Cu plate was underestimated by 35% because of the fluctuation of sensitivity of detector.

By analyzing the resonance dip of ^{107}Ag (E_R: 16.3 eV) and ^{118}Sn (E_R: 45.75 eV) in transmission spectra, the distributions of atomic density of each nuclide were obtained. Fig. 9 shows the cross-section of density distribution for ^{107}Ag and ^{118}Sn. We succeeded in mapping the difference of thickness of sample using the neutron resonance transmission.

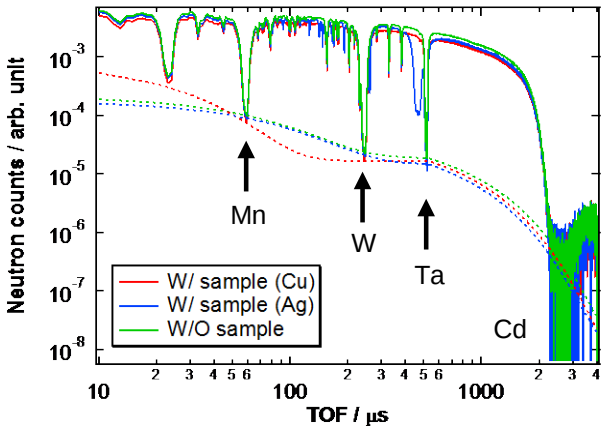

Fig. 8 TOF spectra of neutrons transmitted through the filter (solid) and background curves (dash).

1. 研究成果概要（つづき） Outline of experimental results (continued).

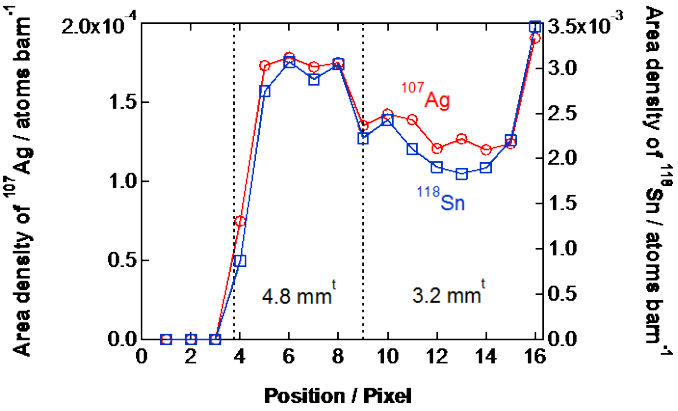

Fig. 9 Cross-section of density distribution of ^{107}Ag and ^{118}Sn.

III. Magnetic field imaging

III. 1 Quantitative magnetic imaging of AC field in a solenoid coil

(1) Experiment

Magnetic imaging experiments using polarized pulsed neutron beam were performed at BL10 “NOBORU”. The experimental setup was the same as the previous experiment. An AC magnetic field was produced by applying a sinusoidal AC electric current, whose amplitude was 1.5 A, to a small solenoid coil with the diameter of 5 mm and length of about 50 mm. A direction of the AC field was arranged to be X direction that is perpendicular to both polarization direction of neutrons (Y direction) and a traveling direction of the pulsed neutron beam (Z direction). To quantify an AC magnetic field, it is necessary to know the phase of applied AC field in which polarized neutrons passed through at a sample position. Therefore, we recorded the time t_0 at which phase of AC field becomes 2π, as an event data together with the neutron event and neutron generation time. Then we calculated the AC phase in which each neutron traversed using t_0, TOF of each neutron event and the distances between the neutron source and the sample coil or the detector. A distance between neutron source and the sample was 13.8m, and the detector was 14.5m.

At first, we tried to measure an AC magnetic field around 50 Hz, which is the frequency of commercial power supply. To analyze AC magnetic field, whose frequency is near the pulsed neutron repetition of J-PARC 25 Hz, the AC field frequency should not be integer multiple of 25Hz, because the relation between AC phase and TOF of neutrons is uniquely determined. In such a case, we cannot analyze the wavelength dependence of the polarization for each phase. To avoid such a problem, the frequency was set to slightly higher than that of a two-fold repetition of the pulsed neutron of J-PARC, 52.5 Hz.

(2) Preliminary Result

Fig. 10 shows the obtained polarization images for various phases with a neutron wavelength of 4.2 Å. Apparent changes of polarization have observed at the position of the sample coil and periodic change of strength of AC magnetic field depending on its phase as observed. Fig. 11 shows the wavelength dependence of polarization at the center of the coil at each phase. A sinusoidal oscillation of polarization against neutron wavelength was observed and its frequency was dependent on the phase. Fig. 12 shows an integrated field strength, estimated from a frequency of the polarization oscillation, plotted against the AC phase. The sinusoidal waveform of the AC field was clearly confirmed and estimated values almost corresponded with that expected from the applied AC current.

Then, we tried to evaluate the strength of much higher frequency field over 500 Hz. In such a case, it is not necessary to avoid integer multiple frequencies of 25Hz as an AC field frequency, because a same phase repetitively appears in a single frame of a pulsed neutron. Therefore, the frequency of AC current was set to 512.5 Hz and 1.0 kHz and the same amplitude of the AC current as previous experiments was applied to the sample coil.

1．研究成果概要（つづき） Outline of experimental results (continued).

Fig. 13 shows the results of integrated field strength at the center of the coil plotted against its AC phase with frequency of 512.5 Hz and 1.0kHz. As can be seen from the figures, we successfully represented the oscillation of higher frequency AC field with almost same precision as the result of 52.5 Hz. Consequently, it is confirmed that this analysis method is adoptable in the quantification of AC magnetic fields with high frequency up to 1 kHz.

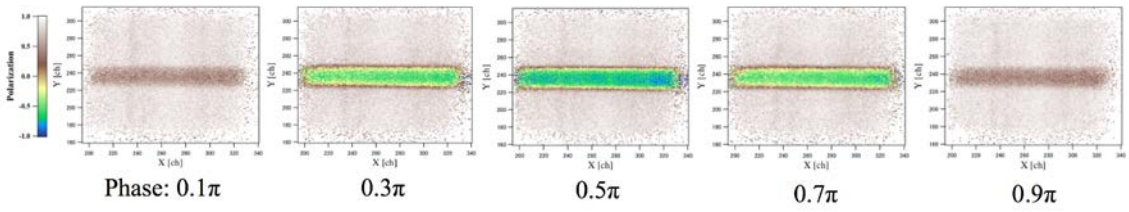

Fig. 10 Polarization distribution images obtained for various AC phases.

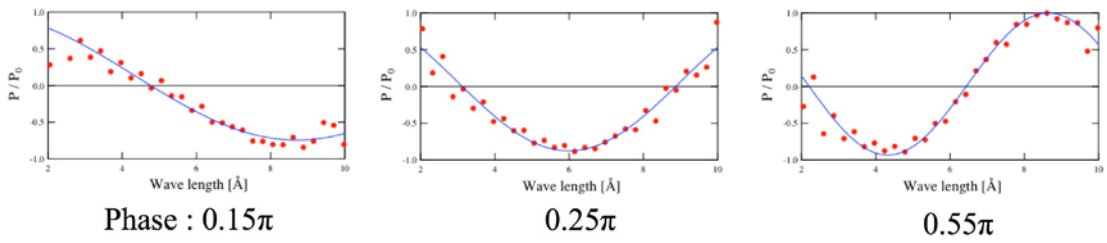

Fig. 11 Wavelength dependence of polarizations obtained for several AC phases. The solid line indicates the results of fitting.

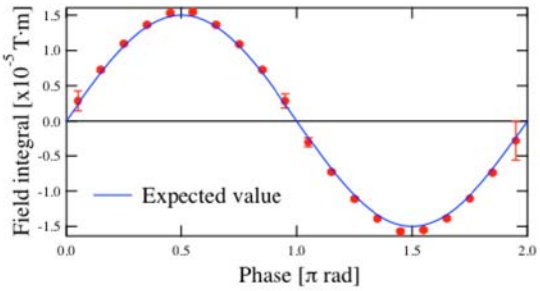

Fig. 12 AC phase dependence of the integrated field strength. The solid line is the field strength expected from the applied AC current.

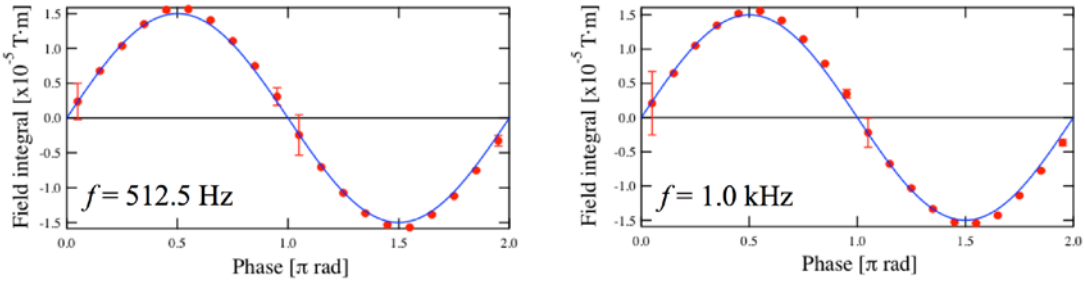

Fig. 13 AC phase dependence of the integrated field strength obtained for the frequency of 512.5 Hz and 1.0kHz.

III. 2 Quantitative imaging of a field direction in a model electric motor

(1) Experiment

Field strength in a model electric motor is so strong that oscillation in wavelength dependence of polarization cannot be observed due to the coarse wavelength resolution of the present experimental setup, and it is difficult to quantify field strength in the motor. Then, we tried to quantify field direction in the motor by changing the direction of quantized axis of a neutron spin using spin-rotators and analyzing the change of polarization degree depending on polarization direction.

Fig. 14(a) shows a schematic picture of the experimental setup at BL10 “NOBORU” and Fig. 14(b) shows a photo of the model motor. The model motor was housing-less structure and the gap distance between a rotor and a stator was about 2 mm. The neutron beam was shaped in 20×20mm^2 by B_4C slits so that rotor and gap were put within a field of view. A μNID was used as a two-dimensional detector and a distance between the source and the detector was 14.78m. We obtained polarization distribution images with changing the direction of quantized axis of polarized neutron beam in 5 steps from Y to X-axis.

(2) Preliminary Result

Fig. 15 shows obtained polarization distribution images. Polarization degree P of polarized neutron that passed through a magnetic field can be expressed as follows,

$$P = 1 - (1 - \langle \cos\varphi \rangle) \cdot \sin^2\theta = \cos^2\theta, \qquad \cdots(1)$$

where φ is a Larmor precession angle and θ is an angle between the magnetic field and the quantized axis of a neutron spin. While the oscillation term, which depends on the precession angle φ, was smeared out due to the coarse wavelength resolution, information about field direction, which corresponds with θ, was still observable in the polarization image taken at each spin-direction. Fig. 16 shows the result of field-direction distribution of the motor. The field in the left and right side of the rotor was aligned along the Y direction and the top and bottom side was along the X direction. Then, we compared this result with that of a computational simulation that calculates field distribution around the model motor. It became clarified that experimentally obtained image is similar to a field distribution of a leakage field around the motor rather than that in the motor. Present analysis model of Eq.(1) assumes that field is uniform in the neutron flight path. For this reason, in case that field distribution changes in a beam path, directional information of the field is overwritten and we can only obtain the information in the most downstream region. To quantify the field distribution in the motor, we have to develop an analysis method that can be applied to a changing field in the beam path.

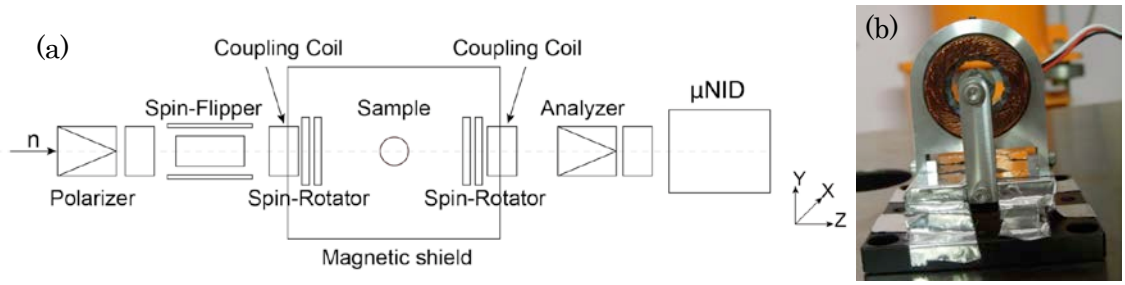

Fig. 14 (a) Schematic picture of the experimental setup (b) Photo of the model electric motor

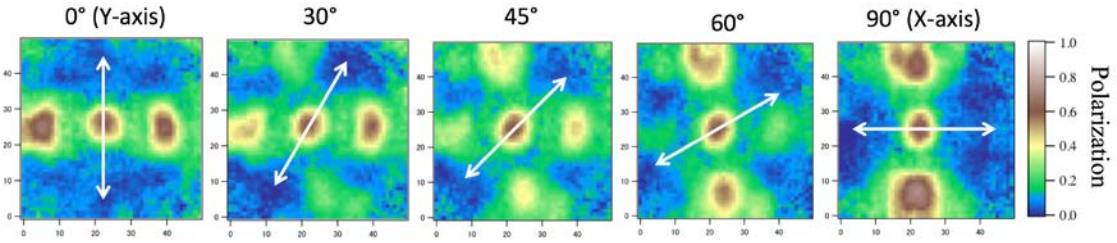

Fig. 15 Obtained polarization distribution images with various direction of quantized axis

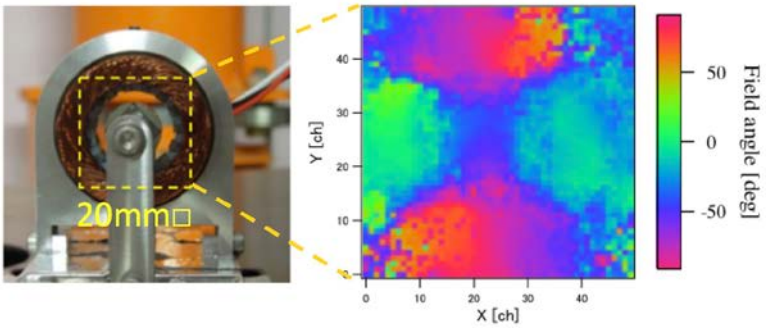

Fig. 16 Distribution image of the field direction

IV. Detector development

IV. 1 The spatial resolution of Image Intensifier.

(1) Background

Camera devices equipped with Image Intensifier (I.I.) enable neutron energy resolved imaging, such as resonance imaging and black-edge imaging. The contrast of the energy-resolved images can be enhanced with use of higher amplification performance of I.I. However, when the amplification performance of I.I. increases, decreases the spatial resolution of obtained images with use of any camera system with I.I.. For related scientific and industrial applications, the fundamental features of camera system coupled with several I.I., such as S/N, spatial resolution and linearity are important information. In this study, a camera system coupled with several high-sensitivity image-intensifiers with the capacity to amplify incident light by more than from 10^4 to about 10^6 was developed. Using several image intensifier which has different capacity to amplify incident light, we evaluated the spatial resolution and detection sensitivity experimentally. In this report, the spatial resolution of the present system coupled with three kinds of I.I. at thermal neutron energy and resonance energy range was shown.

(2) Experiment

The present experimental system was tested at Beam Line 10, J-PARC. Fig. 17 shows a schematic view of the present system set at 13.7 m downstream from the neutron source. The system consists of a neutron scintillator incorporating mixtures of ^{6}LiF/ZnS powder, an optical lens, an I.I., an CCD camera of Andor iKon-L, and a control computer. Three kinds of I.I was prepared, I.I. using a single-stage MCP, a double stage-MCP and double stage-MCP with an image booster. The transmitted neutrons were converted to visible light by a neutron-to-fluorescence scintillator, where the intensity of the emitted light was proportional to the intensity of the entering neutron beam. The 0.1-mm ^{6}LiF/ZnS scintillator was used. The camera sensor comprised 2048 (W) x 2048 (H) pixels. The present system could visualize one TOF image per 40 msec neutron beam cycle. Three kinds of high frame-rate gating type I.I. are allowed us to select the neutron energy with a narrow energy band width of a few μs.

(3) Preliminary Result

First, the spatial resolution at thermal neutron energy range was evaluated with use of a Gd pattern sample. Fig. 18(a-d) show the neutron transmitted ratio images of the Gd sample for CCD without I.I., CCD with I.I of single stage-MCP, CCD with I.I of double stage-MCP, and CCD with I.I of double stage-MCP and image booster. Modulation transfer function (MTF) as a function of spatial frequency was derived as shown in Fig. 19. The spatial frequency at MTF =0.1 was evaluated for CCD without I.I. and CCD with three kinds of MCP, respectively.

Secondly, the spatial resolution at resonance energy region was evaluated by the method of edge spread function. The sample was an Ag sheet of 1 mm in thickness. Fig. 20 shows the neutron transmitted ratio image of the Ag sheet. Using the edge spread function, MTF was evaluated as shown in Fig. 21. We successfully evaluated the spatial resolution at resonance energy region using camera system coupled with several kinds of I.I. The spatial resolution at resonance energy region could be increased if the numbers of incident neutrons increased. Because the J-PARC system is planned to increase by about 2 times from the current neutron flux when approximately 1 MW of acceleration power is achieved, the spatial resolution at resonance energy region may be improved. Further measurements will be carried out to investigate the limit of the spatial resolution of the system as the J-PARC system is powered up.

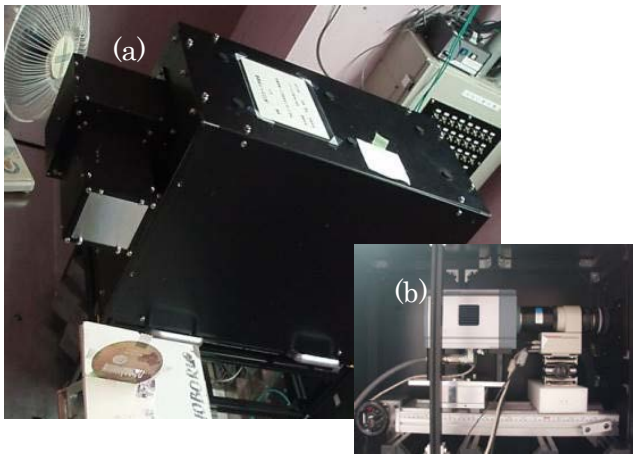

Fig. 17 (a) Experimental set up. (b) Camera system in the black box.

1．研究成果概要（つづき） Outline of experimental results (continued).

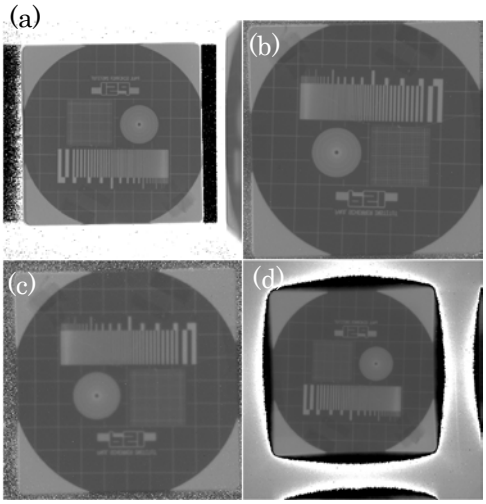

Fig. 18 Neutron transmitted ratio images by (a) CCD (b) CCD with I.I. of single-stage MCP(c) CCD with I.I. of double-stage MCP (d) CCD with I.I. of double-stage MCP and image booster.

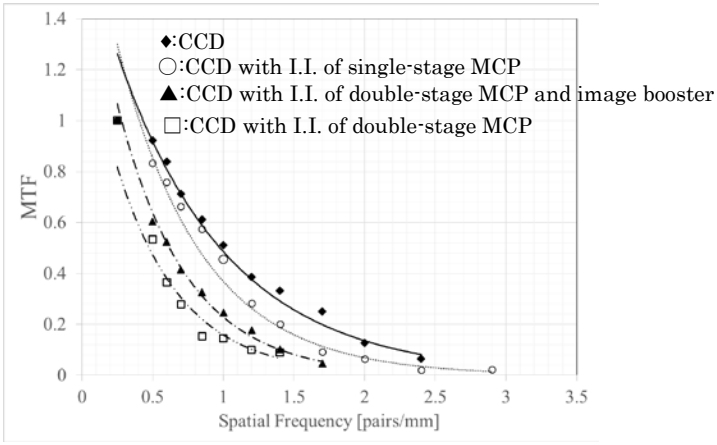

Fig. 19 MTF at thermal neutron energy (preliminary).

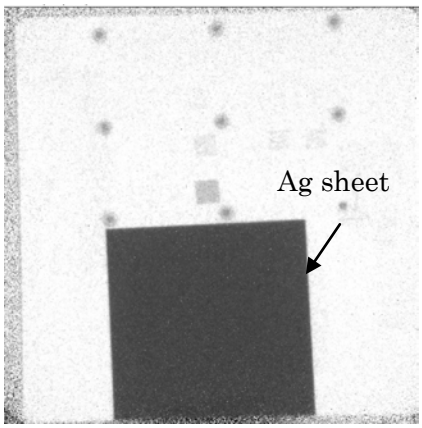

Fig. 20 Neutron transmitted image of Ag sheet

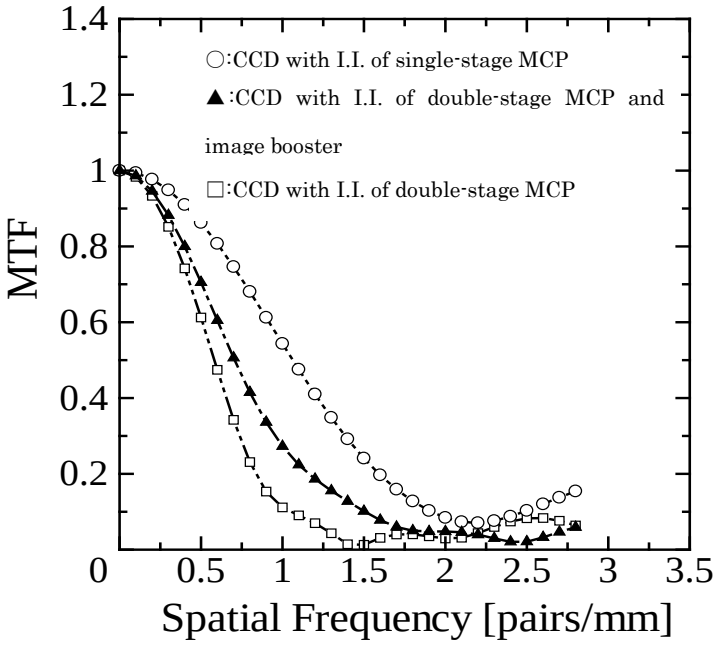

Fig. 21 MTF at resonance neutron energy range (preliminary)